

論文 / 著書情報
Article / Book Information

論題	
Title	Effect of in situ annealed SnO ₂ buffer layer on structural and electrical properties of (001) SnO ₂ /TiO ₂ heterostructures
著者	奥出 正樹, 上野 和紀, 伊藤 俊, 菊池 昌枝, 大友 明, 川崎 雅司
Author	M. Okude, K. Ueno, S. Itoh, M. Kikuchi, A. Ohtomo, M. Kawasaki
掲載誌/書名	, Vol. 41, No. 12, 125309-1-4
Journal/Book name	Journal of Physics D-Applied Physics, Vol. 41, No. 12, 125309-1-4
発行日 / Issue date	2008, 5
Note	このファイルは著者（最終）版です。 This file is author (final) version.

Effect of *in-situ* annealed SnO₂ buffer layer on structural and electrical property of (001) SnO₂/TiO₂ heterostructures

Masaki Okude¹, Kazunori Ueno¹, Sun Itoh¹, Masae Kikuchi¹, Akira Ohtomo¹, and Masashi Kawasaki^{1,2}

¹ *Institute for Materials Research, Tohoku University, Sendai 980-8577, Japan*

² *WPI Advanced Institute for Materials Research and Institute for Materials Research, Tohoku University, Sendai 980-8577, Japan*
CREST, Japan Science and Technology Agency, Tokyo 102-0075, Japan

Electronic mail: okude@imr.tohoku.ac.jp

Abstract

We have studied heteroepitaxial growth of SnO₂ films on (001) TiO₂ substrates by pulsed laser deposition. In order to reduce crystalline defects arising from a large lattice mismatch (3.1%), SnO₂ buffer layer is employed. The buffer layer prepared by *in-situ* annealing at an optimized condition exhibits atomically flat surface and partially relaxed lattice, which play an important role in the improvement of crystallinity and electrical property for the overgrown layer. The results are discussed based on the structural characterization by means of x-ray diffraction and transmission electron microscopy and temperature dependence of Hall mobility.

1. Introduction

Transparent conducting oxides (TCO) attract increasing interests for practical application such as flat panel displays and solar cells. Recent markup of indium due to limited resources and rapidly expanding demands emerge a new technological challenge for replacing In_2O_3 -based TCO by other materials [1]. More abundant choices are ZnO and SnO_2 , which can be, in principle, employed as heavily doped and degenerated semiconductors [2]. Usually, a carrier concentration of over 10^{21} cm^{-3} and a mobility of over $10 \text{ cm}^2\text{V}^{-1}\text{s}^{-1}$, yielding in a conductivity greater than 10^3 Scm^{-1} , are of interest. The carrier concentration can be controlled by dopant concentration in any form of the films from single crystalline, through texture to polycrystalline, but the mobility strongly depends on the crystallinity, although screening effect smears carrier scattering for heavily doped metallic states. For increasing the conductivity, thus it is important to elucidate the intrinsic mobility of the materials.

Among them, the intrinsic characteristics are best studied in ZnO. Hall mobility (μ_{H}) of $440 \text{ cm}^2\text{V}^{-1}\text{s}^{-1}$ was demonstrated at 300 K for a single crystalline thin film with electron concentration of $9 \times 10^{15} \text{ cm}^{-3}$, which was grown on $\text{Mg}_x\text{Zn}_{1-x}\text{O}$ buffer layer on a lattice-matched substrates [3]. Single crystalline In_2O_3 films were prepared on nearly lattice-matched (111) YSZ substrate to record μ_{H} of $110 \text{ cm}^2\text{V}^{-1}\text{s}^{-1}$ at 300 K for a film with electron concentration of $7 \times 10^{18} \text{ cm}^{-3}$ [4]. These high-quality epilayers usually show a bell-shaped temperature dependence of μ_{H} , where the mobility first increases with lowering temperature due to suppression of phonon scattering and then declines due to impurity scattering as the carriers rapidly freeze out.

A bulk SnO_2 single crystal has the highest mobility among rutile-type oxide ($\mu_{\text{H}} = 240 \text{ cm}^2\text{V}^{-1}\text{s}^{-1}$ at 300 K) [5]. There have been reported many studies of SnO_2 texture films grown on such substrates as *r*-plane sapphire [6] and (100) TiO_2 [7]. However, temperature dependence of the electrical properties has not yet been investigated. Therefore, it is interesting to examine the electrical properties for an epitaxially grown SnO_2 film.

In this study, we employ (001) rutile TiO₂ substrates. Its crystal structure is identical to that of SnO₂ and the lattice mismatch is 3.1% along the [100] direction and 7.7% along the [001] direction, respectively. In order to minimize the influence of lattice mismatch, we show that the use of *in-situ* annealed SnO₂ buffer layer is an effective way of reducing the defect extending from the substrate/film interface to the SnO₂ layer, yielding in a low-temperature μ_{H} substantially higher than that of as-grown films.

2. Experimental

The films were deposited on (001) TiO₂ substrates by pulsed laser deposition. A SnO₂ ceramic target (99.99% purity), placed 45 mm away from the substrate surface, was ablated with KrF excimer laser pulses at a repetition of 10 Hz and at a fluence of 1.5 J/cm². The substrates were etched in 23% HF aqueous solution and annealed at 1100°C for 12 hours in air prior to the film deposition in order to prepare atomically flat surface [8]. Approximately 100 nm-thick films were deposited (hereafter denoted as as-grown) at 540°C and at an oxygen pressure (P_{O_2}) of 1×10^{-3} Torr. Some of the as-grown films were annealed at 750°C or 800°C in $P_{\text{O}_2} = 1 \times 10^{-8}$ Torr for 1 hour and then annealed in 1 atm of oxygen gas at 400°C in the deposition chamber (denoted as 750°C-annealed and 800°C-annealed, respectively). The overgrowth layers of SnO₂ were prepared on the 750°C-annealed films with a thickness of 30 nm (denoted as overgrown).

The crystallinity of the films was characterized by a powder x-ray diffraction (XRD) apparatus (Rigaku, RINT-RAPID) and a high-resolution four-circle XRD apparatus (Philips, X'-pert MRD). The film surface was characterized by reflection high-energy electron diffraction (RHEED) and atomic force microscopy (AFM). The electrical properties were measured by Quantum Design PPMS. Cross-sectional transmission electron microscopy (TEM, JEM-2000EX2 operated at 200 kV) observation was also carried out to characterize defect structure in the heterostructures.

3. Results and discussion

We first optimized the deposition conditions of SnO₂ film by varying growth temperature from 450°C to 650°C and P_{O_2} from 1×10^{-6} Torr to 1×10^{-2} Torr. Except for the films grown in 1×10^{-3} Torr, RHEED patterns showed 3D-growth mode and the AFM image indicated rough surface. For the films grown in 1×10^{-3} Torr, a weak streak RHEED pattern and smooth surface were obtained at growth temperature of 540°C, although step and terrace structures were not clearly observed in the AFM image [Figure 1 (a) and (e)]. Next, we carefully sought an optimal annealing condition for preparing excellent buffer layer. In order to improve surface flatness, we first rose temperature up to 800°C while maintaining P_{O_2} set at growth condition, *i.e.*, 1 mTorr, but RHEED pattern remained unchanged. By decreasing P_{O_2} to 1×10^{-8} Torr, the surface became much smoother. The 750°C-annealed film showed a fine streak RHEED pattern [Figure 1(b)] and step and terrace structures in AFM image [Figure 1(f)]. However, the 800°C-annealed film had apparently rough surface as shown in the AFM image [Figure 1(g)] and spotty RHEED pattern [Figure 1(c)]. Therefore, an optimal annealing condition for the buffer layer was set as 750°C in $P_{O_2} = 1 \times 10^{-8}$ Torr. Indeed, the atomically flat surface was kept after overgrowth of SnO₂ film on the buffer layer [Figure 1(d) and (h)]. The similar effect of annealed buffer layers has been confirmed for Ba_{0.5}Sr_{0.5}TiO₃ [9] and ZnO [10] heteroepitaxial films. Another annealing step in 1 atm of oxygen was followed in order to annihilate oxygen vacancies in the film and substrates.

Figure 2(a) shows XRD pattern of the as-grown film. The strong (002) peak indicates that the film was epitaxially grown along the substrate orientation. Figure 2(b) shows a reciprocal space mapping of the asymmetric (112) peak for the same film. From the peak position, $d_{110} = 3.331 \text{ \AA}$ and $d_{002} = 1.599 \text{ \AA}$ are extracted, which indicate that the lattice is elastically strained with a compression along the in-plane by ~0.6% with respect to bulk SnO₂ ($d_{110} = 3.350 \text{ \AA}$ and $d_{002} = 1.593 \text{ \AA}$). In fact, d_{110} and d_{002} change systematically as shown in the inset of figure 2(b) for all the films, to which a linear fit gives a slope of

0.67 that is close to the value calculated from elastic stiffness constants as $C_{13}/C_{33} = 0.69$ [11]. As for 750°C-annealed and overgrown films, the film lattice was relaxed to $d_{110} = 3.336 \text{ \AA}$ and $d_{002} = 1.598 \text{ \AA}$. The 800°C-annealed film is less strained ($d_{110} = 3.340 \text{ \AA}$ and $d_{002} = 1.596 \text{ \AA}$), suggesting that annealing at much higher temperature will allow to accommodate a strain-free buffer layer. The compromise with surface roughening effect prohibits further increase of annealing temperature on achievement of the fully relaxed buffer layer.

We further analyzed the reciprocal space mapping data to extract the lateral grain size. The lateral grain size appears inversely proportional to peak spread along the in-plane direction (the [110] direction in this case) [12]. For instance, the film peak seen in figure 2(b) has broader profile along the horizontal axis. By measuring the full width at half maximum, we obtain lateral grain size of $90 \pm 20 \text{ nm}$ for the as-grown film, and also $220 \pm 30 \text{ nm}$ and $60 \pm 20 \text{ nm}$ for the overgrown and 800°C-annealed films, respectively (data not shown). Although the evaluation of grain size is inaccurate given the effect of strain on spread width of the diffraction peak, the improved crystalline quality could be further verified by observing cross-section TEM for as-grown and overgrown SnO₂ films as shown in figure 3. In the TEM image of the as-grown film, there can be seen dense defects near the interface, which extend to the surface. However, most of defects were congregated only in the buffer layers in annealed buffer layer and rather low density of defects extends to the overgrown layer.

Now, we compare the electrical properties of the films. Figure 4 shows the temperature dependence of conductivity (σ) and Hall mobility measured for three representative films discussed so far. μ_{H} of as-grown film at 300K is $36 \text{ cm}^2\text{V}^{-1}\text{s}^{-1}$, which is comparable to nominally undoped films grown on sapphire substrates [6] whereas the carrier density is as low as $1.0 \times 10^{18} \text{ cm}^{-3}$, which is notably lower than that grown on the sapphire substrates by an order of magnitude. The overgrown SnO₂ film has a comparable μ_{H} at 300K with the as-grown film but increases its value up to $38 \text{ cm}^2\text{V}^{-1}\text{s}^{-1}$ at 200K, representing bell-shaped temperature dependence. The 750°C-annealed film had much lower μ_{H} and σ

than those of as-grown and overgrown films. Therefore, we conclude that the annealing process degrades the electron mobility but overgrown layer has much better quality than that as-grown film. In fact, a thicker as-grown film (200 nm) indicated essentially no difference in electrical properties with respect to the 100-nm-thick as-grown film, which excludes mere thickness dependence, but confirms the effect of buffer layer. When we compare the results of figures 3 and 4 with the film grown on sapphire substrates [6] we presume that different carrier concentration arises from their own intrinsic defects. Since annealed buffer layer reduces defects extended to the overgrown layer, mobility is enhanced at low temperatures.

4. Conclusions

We have demonstrated the effect of annealed SnO₂ buffer layer on the improved crystalline quality and electrical properties of overgrown SnO₂ films on (001) TiO₂ substrates. We find an optimum annealing condition of the buffer layer to achieve atomically flat surface and partially relaxed lattice, both of which are required to improve structural and electrical properties of overgrown layer. The peak mobility of 38 cm²V⁻¹s⁻¹ is recorded at 200 K for the film grown on the buffer layer annealed at 750°C.

References:

- [1] Minami T 2005 Transparent conducting oxide semiconductors for transparent electrodes *Semicond. Sci. Technol.* **20** S35
- [2] Zhang D H and Ma H L 1996 Scattering mechanisms of charge carriers in transparent conducting oxide films *Appl. Phys. A* **62** 487
- [3] Tsukazaki A, Ohtomo A and Kawasaki M 2006 High-mobility electronic transport in ZnO thin films *Appl. Phys. Lett.* **88** 152106
- [4] Koida T and Kondo M 2006 High electron mobility of indium oxide grown on yttria-stabilized zirconia *J. Appl. Phys.* **99** 123703
- [5] Fonstad C G and Rediker R H 1971 Electrical properties of high-quality stannic oxide crystals *J. Appl. Phys.* **42** 2911
- [6] Dominguez J E, Pan X Q, Fu L, Van Rompay P A, Zhang Z, Nees J A and Pronko P P 2002 Epitaxial SnO₂ thin films grown on ($\bar{1}012$) sapphire by femtosecond pulsed laser deposition *J. Appl. Phys.* **91** 1060
- [7] Wakabayashi H, Suzuki T, Iwazaki Y and Fujimoto M 2001 Defect structure of heteroepitaxial SnO₂ thin films grown on TiO₂ substrates *Jpn. J. Appl. Phys.* **40** 6081
- [8] Yamamoto Y, Nakajima K, Ohsawa T, Matsumoto Y and Koinuma H 2005 Preparation of atomically smooth TiO₂ single crystal surfaces and their photochemical property *Jpn. J. Appl. Phys.* **44** L511.
- [9] Terai K, Lippmaa M, Ahmet P, Chikyow T, Fujii T, Koinuma H and Kawasaki M 2002 In-plane lattice constant tuning of an oxide substrate with Ba_{1-x}Sr_xTiO₃ and BaTiO₃ buffer layers *Appl. Phys. Lett.* **80** 4437.
- [10] Tsukazaki A, Ohtomo A, Yoshida S, Kawasaki M, Chia C H, Makino T, Segawa Y, Koida T, Chichibu S F and Koinuma H 2003 Layer-by-layer growth of high-optical-quality ZnO film on atomically smooth and lattice relaxed ZnO buffer layer *Appl. Phys. Lett.* **83** 2784.

- [11] Hazen R M and Finger L W 1981 Bulk moduli and high-pressure crystal structures of rutile-type compounds *J. Phys. Chem. Solids*, **42** 143
- [12] Ohtomo A, Kimura H, Sato K, Makino T, Segawa Y, Koinuma H and Kawasaki M 2000 Lateral grain size and electron mobility in ZnO epitaxial films grown on sapphire substrates *J. Cryst. Growth* **214/215** 284

Figure captions:

Figure 1. RHEED pattern for (a) as-grown, (b) 750°C-annealed, (c) 800°C-annealed, and (d) overgrown SnO₂ films. Corresponding AFM images (2 μm x 2 μm) to (a)~(d) are shown in (e)~(h), respectively.

Figure 2. (a) x-ray diffraction pattern of as-grown film on (001) TiO₂ substrate. (b) Reciprocal space mapping around the asymmetric (112) diffraction peaks for the same sample. The cross stands for the peak position expected for bulk SnO₂. The inset depicts the values of d_{110} and d_{002} for various films described in text.

Figure 3. Cross-section transmission electron microscopy images of as-grown (left) and overgrown SnO₂ (right) films.

Figure 4. Temperature dependence of (a) conductivity σ and (b) Hall mobility μ_H for three representative films. n_{300K} is free electron concentration at 300 K.

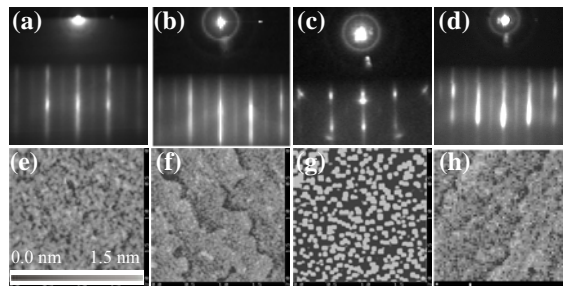


Figure 1. RHEED pattern for (a) as-grown, (b) 750°C-annealed, (c) 800°C-annealed, and (d) overgrown SnO₂ films. Corresponding AFM images (2 μm x 2 μm) to (a)~(d) are shown in (e)~(h), respectively.

Figure 1. M. Okude *et al.*

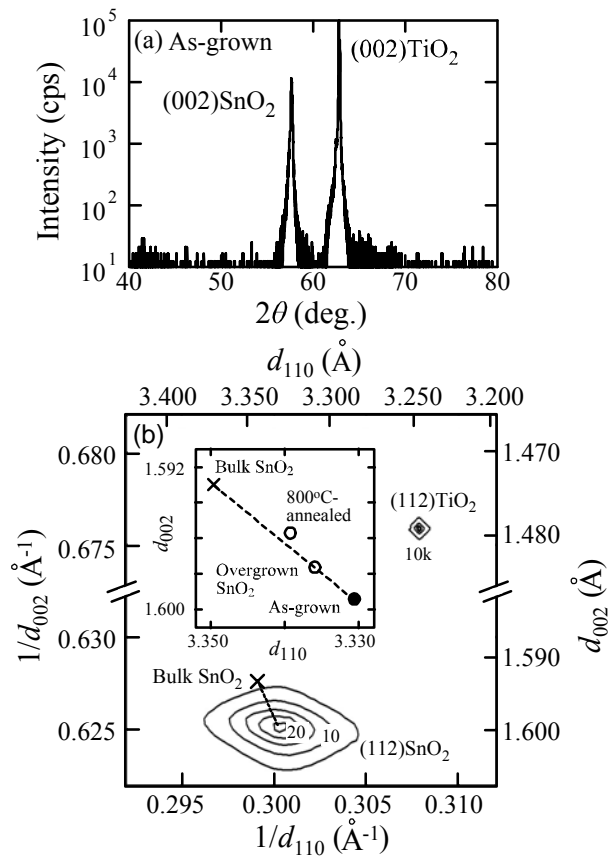


Figure 2. (a) x-ray diffraction pattern of as-grown film on (001) TiO_2 substrate. (b) Reciprocal space mapping around the asymmetric (112) peaks for the same sample. The cross marks to the peak position expected for bulk SnO_2 . The inset depicts the values of d_{110} and d_{002} for various films described in text.

Figure 2. M. Okude *et al.*

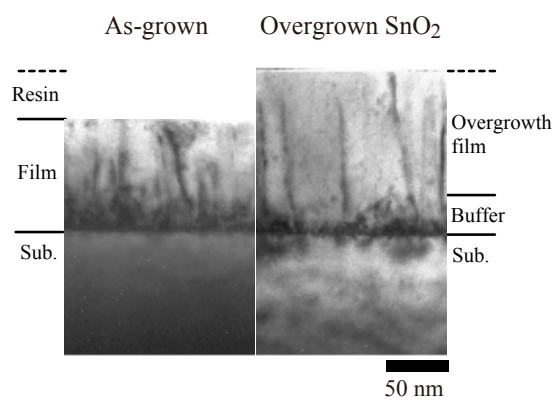


Figure 3. Cross-section transmission electron microscopy images of as-grown (left) and overgrown SnO₂ film (right).

Figure 3. M. Okude *et al.*

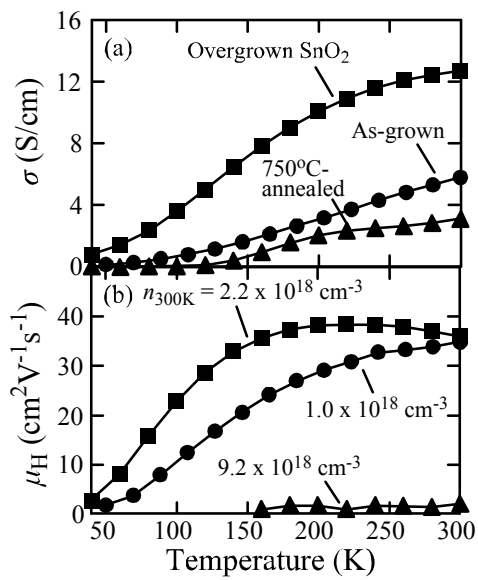


Figure 4. Temperature dependence of (a) conductivity σ and (b) Hall mobility μ_H for three representative films. n_{300K} is free electron concentration at 300 K.

Figure 4. M. Okude *et al.*